

CHAPTER 3

CHARACTERISATION STUDIES ON CdI₂ DOPED

Ag₂O-V₂O₅- B₂O₃ SYSTEM

This chapter discusses the characterization studies. The samples obtained were pulverized and characterized by X-ray diffraction, Differential Scanning Calorimetry, Fourier transform Infra-red Spectrometry, Transport number measurements by Wagner's polarization method and emf technique, Thermo electric Power measurements etc.

3.1. X-ray Diffraction

X-rays are electromagnetic radiation with typical photon energies in the range of 100 eV-100 keV. For diffraction applications, only short wave length x-rays (hard x-rays) in the range of few angstroms to 0.1 angstroms (1keV-120 k eV) are used. Because the wave length of x-rays is comparable to the size of atoms, they are ideally suited for probing the structural arrangement of atoms and molecules in a wide range of materials. The energetic x-rays can penetrate deep into the materials and provide information about the bulk structure.

X-rays are produced generally by x-ray tubes, where an electron beam, accelerated across a high voltage field, bombards a stationary or rotating solid target. As electrons collide with atoms in the target and slow down, a continuous spectrum of x-rays is emitted, which is termed as Bremsstrahlung radiation. The high energy electrons also eject inner shell electrons in atoms through the ionization process. When a free electron fills the shell, an x-ray photon with energy characteristics to the target material is emitted. Common

target used in x-ray tubes include Cu and Mo, which emit 8 keV and 14 keV x-rays with corresponding wavelength of 1.54 Å and 0.8 Å, respectively.

Diffraction occurs as waves interact with a regular structure whose repeat distance is about the same as wavelength of x-rays. It happens when x-rays have wavelength of the order of few angstroms which is the same as the typical inter atomic distance in crystalline solids. Diffracted waves from different atoms can interfere with each other and the resultant intensity distribution is strongly modulated by this interaction. In crystals, the diffracted waves will consist of sharp interference maxima (peaks) with the same symmetry as in the distribution of atoms. Obtained diffraction pattern, therefore, allow us to deduce the distribution of atoms in a material.

The peaks in the diffraction pattern are directly related to the atomic distance. For a given set of lattice plane with an inter planar distance of d , the condition of diffraction is given by Bragg's law as, $n\lambda=2d\sin\theta$, where λ is the wave length in angstrom (1.54 Å for Cu), d is the inter atomic spacing in angstroms, θ is the diffraction angle in degrees and n is the integer representing the order of the diffraction peak.

X-ray diffraction measurements were carried out in order to determine the amorphous state of the present samples. Absence of well defined peak in the x-ray diffraction spectra characterizes the glassy state [1-2]. In the first series, $x\text{CdI}_2\text{-(100-x)} [2\text{Ag}_2\text{O-(0.7V}_2\text{O}_5\text{-0.3B}_2\text{O}_3)]$, the amount of CdI_2 is changing from 5 to 30 in steps of 5. Fig. 3.1 shows the X-ray spectrum obtained for the samples of the first series at room temperature. The observed featureless patterns showed the absence of crystalline phases only for those samples with $x = 15$ to 25. The rest of the samples exhibited the presence of some peaks even after they are prepared by fast quenching technique. For the samples

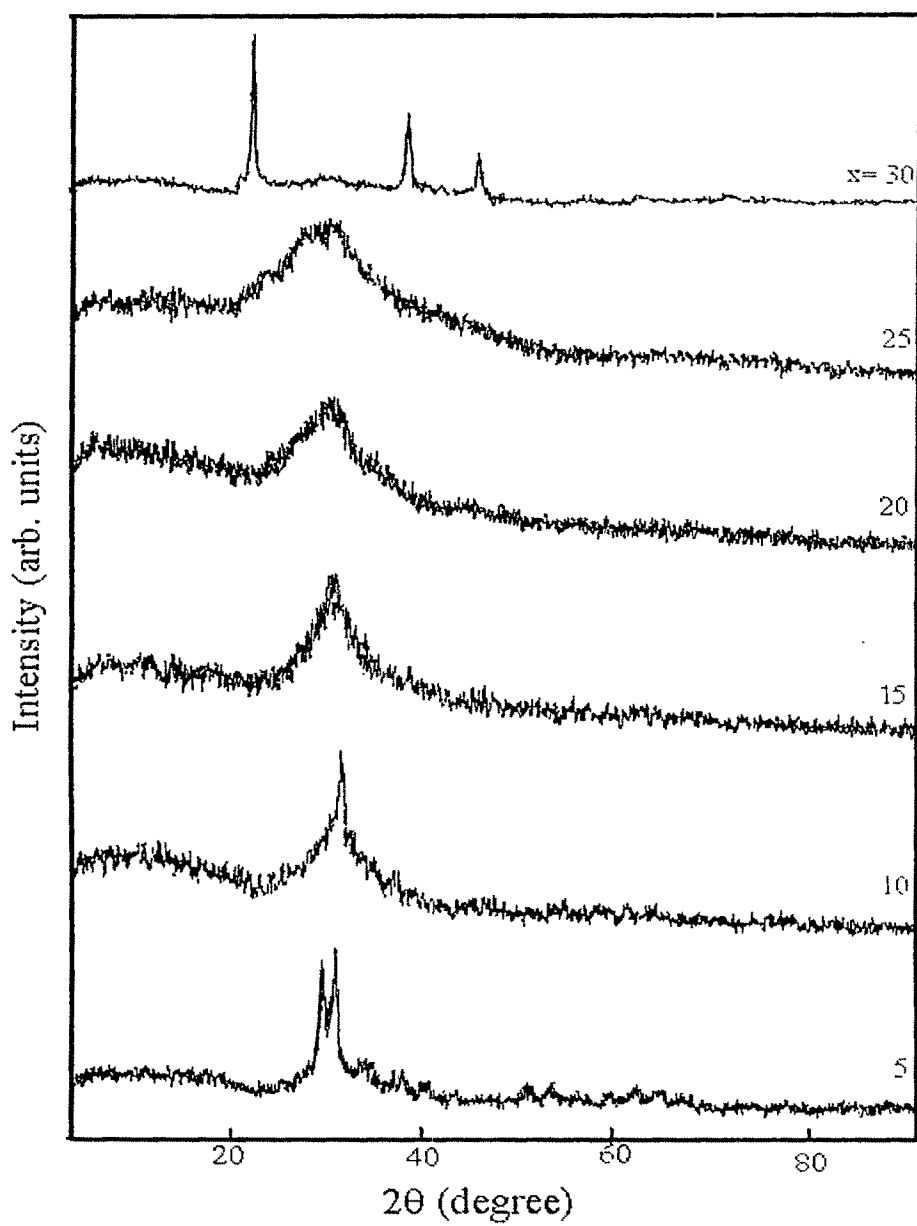


Fig.3.1 X-ray spectrum obtained at room temperature for the series $x\text{CdI}_2-(100-x)[2\text{Ag}_2\text{O}-(0.7\text{V}_2\text{O}_5-0.3\text{B}_2\text{O}_3)]$ where $5 \leq x \leq 30$.

with $x = 5$ and 10 the x-ray spectrum shows an amorphous background with a peak at $2\theta = 31.8^\circ$ and it may be due to the agglomeration of Ag_2O in the system. For the sample with $x=30$, shows the x-ray spectrum having an amorphous background with peaks due to $\beta\text{-AgI}$ at $2\theta = 23.5^\circ$, 39.0° and 46.1° . In silver iodide, iodide ions are known to form a mixture of closely packed structures at temperature well below 147°C consisting of fcc and hcp structures which are commonly designated as $\gamma\text{-AgI}$ and $\beta\text{-AgI}$ respectively. The appearance of these peaks in the x-ray spectrum of 30 mole% of CdI_2 composition has been attributed to the presence of AgI in the system and is due to the exchange reaction between Cd^{2+} and Ag^+ in the system. Similar features have been observed for 30 mole% of PbI_2 doped $\text{Ag}_2\text{O-V}_2\text{O}_5$ system [3].

In the second series, $20\text{CdI}_2\text{-}80[x\text{Ag}_2\text{O-y}(0.7\text{V}_2\text{O}_5\text{-}0.3\text{B}_2\text{O}_3)]$ where the ratio of the amount of modifier to former, x/y is changed between 1 to 3 in steps of 0.25 and the dopant is kept constant. Fig.3.2 shows the x-ray spectra obtained for the samples of series two. The x-ray diffraction spectra of the samples with x/y ratio 1.5, 1.75 and 2 show a peak free diffraction pattern. The samples with $x/y = 2.25$ to 3 show an amorphous background with peaks due to Ag_2O at around $2\theta = 31.9^\circ$ which may be due to the agglomeration of Ag_2O within the mixed system. The sample with $x/y = 1.25$ is found to be a mixture of glass and polycrystalline and $x/y = 1$ is a polycrystalline one. The observed diffraction spectrum for $x/y = 1$ and 1.25 suggests the presence of AgI as well as some unidentified phases probably due to the reaction between Ag_2O , V_2O_5 , B_2O_3 and CdI_2 . The observed peaks obtained at $2\theta = 22.8^\circ$, 23.5° , 38.3° and 46.6° show the presence of AgI in the system. The observed peak at $2\theta = 60.2^\circ$ and 65.9° show the presence of CdO_2 and CdO in the samples with $x/y = 1$ and 1.25. Thus the limit of glass formation has been set at

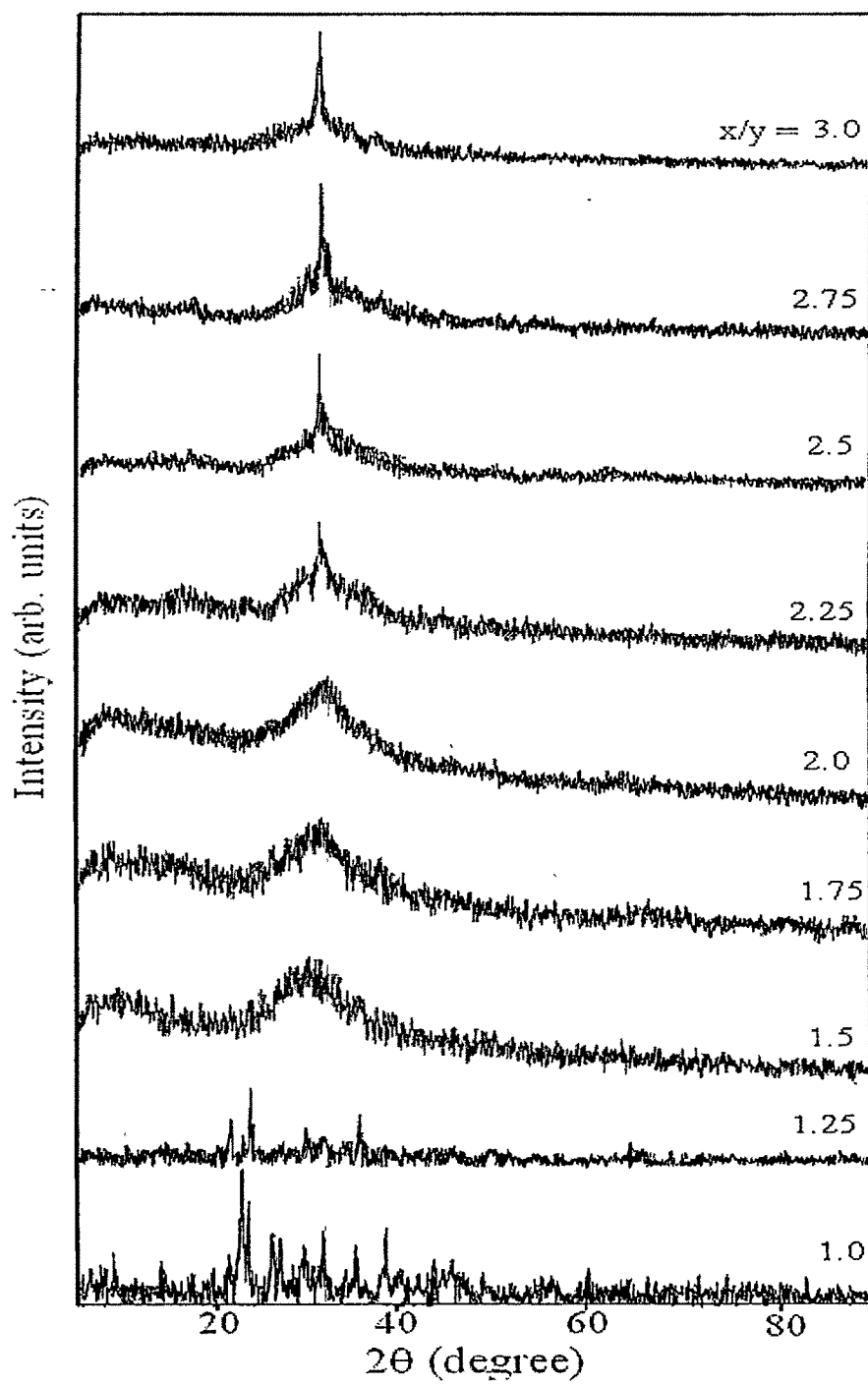


Fig.3.2 X-ray spectrum obtained at room temperature for the second series $20\text{CdI}_2\text{-}80[x\text{Ag}_2\text{O-y}(0.7\text{V}_2\text{O}_5\text{-}0.3\text{B}_2\text{O}_3)]$ where $1 \leq x/y \leq 3$.

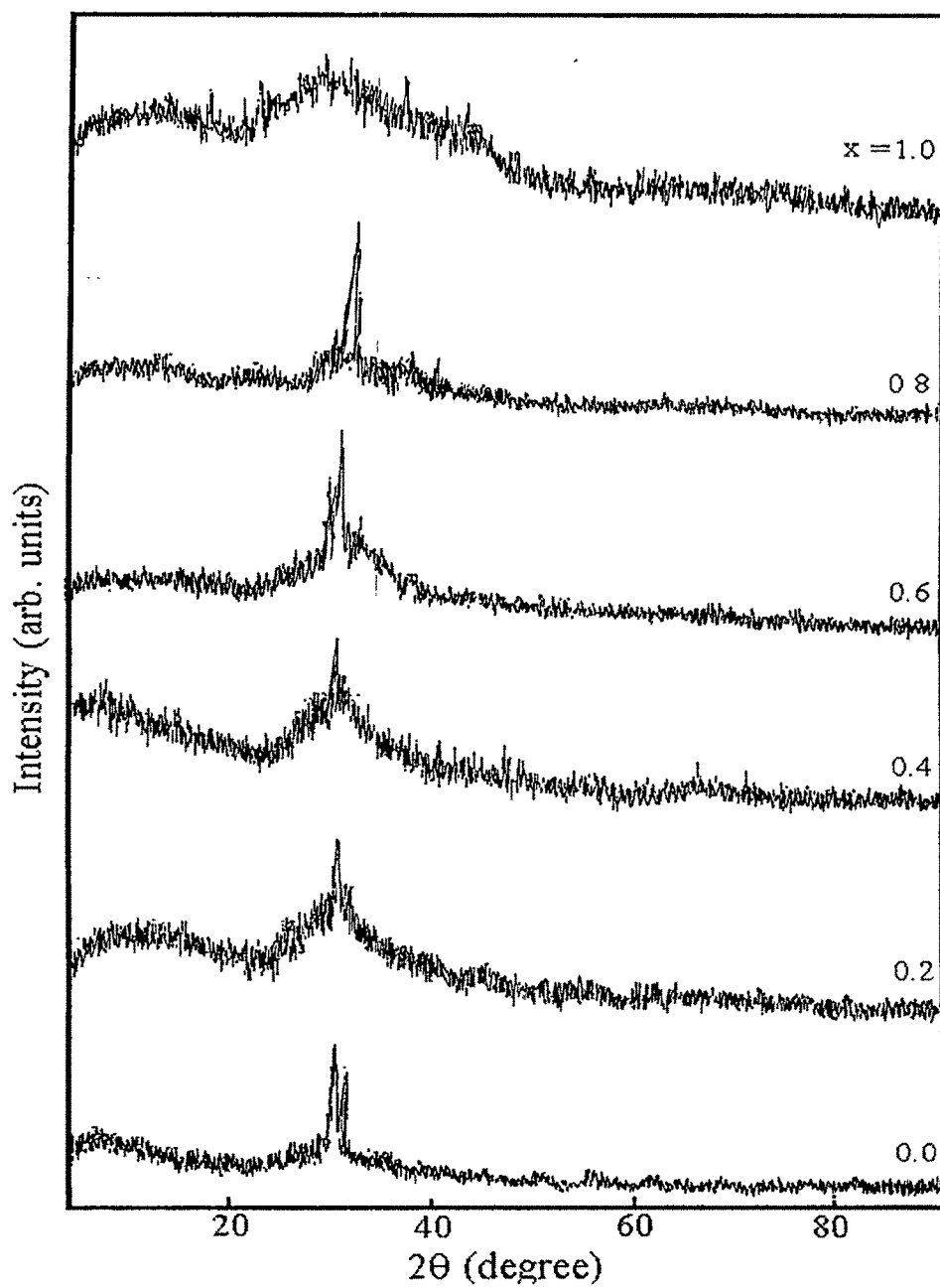


Fig.3.3 X-ray spectrum obtained at room temperature for the third series $20\text{CdI}_2\text{-}53.4\text{Ag}_2\text{O-}26.6[\text{xV}_2\text{O}_5\text{-(1-x)B}_2\text{O}_3]$

$1.5 \leq x/y \leq 3$.

In the third series, $20\text{CdI}_2\text{-}53.4\text{Ag}_2\text{O-}26.6[\text{xB}_2\text{O}_3\text{-(1-x)V}_2\text{O}_5]$, where the amount of dopant CdI_2 and modifier Ag_2O is constant and one of the glass former (V_2O_5) is replaced by another (B_2O_3) in steps of 0.2. Fig.3.3 shows the x-ray spectra obtained for the samples of series three. All the samples show the peak due to Ag_2O which may be due to the agglomeration of Ag_2O in the system. Some traces of silver aggregates may be present in the sample for $x=0$. The peaks obtained at 38° , 44.1° and 65° could be attributed to the presence of metallic silver. The formation of unidentified new phases is inferred from the peaks at $2\theta = 33.3^\circ$, 45.1° , 55.2° , 57.1° , 61.4° etc. The presence of AgI phase is seen from the peaks observed at $2\theta = 39.2^\circ$ for $x=0.4$, 0.8 and 1 .

From the above discussion it is clear that out of these materials some have agglomerates (crystallites) of AgI , Ag , CdO_2 , CdO and some other new phases which are remain undissolved or could not be spread uniformly under given conditions. The x-ray spectrum obtained for all the samples are quite broad in shape thus suggesting its highly disordered nature.

3.2. Differential Scanning Calorimetry

Thermal analysis techniques are a group of methods which are used to determine the physical and chemical properties of materials as a function of temperature or time. In each method, the sample is subjected to a controlled temperature programme, which may involve heating or cooling (dynamic) or holding the temperature constant (isothermal). Thermal analysis techniques include

1. Thermo gravimetric analysis (TGA)

2. Differential thermal analysis (DTA)
3. Differential Scanning Calorimetry (DSC)
4. Dynamic Mechanical Thermal Analysis (DMTA) etc.

The present study has been made using DSC technique of the instrument model DSC2910 Differential Scanning Calorimeter (TA Instrument). It measures the temperature and heat flow associated with transition in materials as a function of time and temperature. Such measurements provide quantitative and qualitative information about physical and chemical changes that involve endothermic or exothermic processes or changes in heat capacity.

In the DSC plot, the X-axis represents the temperature and the Y-axis represents the difference in heat flow between the sample and the reference. When we start heating the sample and reference material, in the DSC apparatus, the computer will plot the difference in heat flow against temperature. That is the heat absorbed or released by the material against temperature. The plot will look as a horizontal line at first, is shown in Fig.2.2. The heat flow is shown in units of heat, q supplied per unit time, t . The heating rate is temperature increase ΔT per unit time, t .

$$\text{Heat flow} = \frac{\text{heat}}{\text{time}} = \frac{q}{t} \quad (3.1)$$

$$\text{Heating rate} = \frac{\Delta T}{t} \quad (3.2)$$

If we divide eqn. (3.1) by (3.2)

$$\frac{q/t}{\Delta T/t} = \frac{q}{\Delta T} = C_p = \text{heat capacity} \quad (3.3)$$

While heating the substance, the amount of heat required to get a certain temperature increase is called the heat capacity. After a certain amount of temperature, the horizontal line in the DSC spectrum shifts downward suddenly, means heat is being absorbed by the sample or a change (increase) in its heat capacity. Because of this change in heat capacity that occurs at the glass transition, DSC is used to measure the substance glass transition temperature. Above the glass transition, the substance has a lot of mobility. When they reach the right temperature, they will have gained enough energy to move into very ordered arrangements, called crystals. When the substance fall into these crystalline arrangements, they give off heat and is seen as an exothermic peak in the plot of heat flow versus temperature. The temperature at the highest point is usually considered to be the substance crystallization temperature, or T_c . The substance gives off heat when it crystallizes; it is called an exothermic transition. After this, it eventually reaches another thermal transition, called melting. At the melting temperature, or T_m , those crystals formed began to fall apart i.e., it starts melting. The chains come out of their ordered arrangements, and begin to move around freely. When the substance crystals melt, they must absorb heat (add energy) in order to do so and melting is a first order transition (endothermic transition). The DSC plot shows a big difference between the glass transition and the other two thermal transitions, crystallization and melting. In glass transition, there is no peak, because there is no latent heat given off, or absorbed, by the substance. Both melting and crystallization involve absorbing or giving off heat. In the glass transition temperature, there is only a change in the heat capacity of the sample. Because there is a change in heat capacity, but there is no latent heat involved with the glass transition, we call the glass

transition a second order transition. Transitions like melting and crystallization, which do have latent heats, are called first order transitions.

In a DSC thermogram, four types of transitions are possible.

1. Second order transition in which a change in the horizontal base line is detected.
2. An endothermic curve peak caused by a fusion or melting reaction.
3. An endothermic curve peak due to a decomposition or dissociation transition
4. An exothermic curve caused by a crystalline phase change.

The number, shape and position of various peaks with reference to the temperature may be used as a means for the qualitative identification of the substance under investigation.

The amorphous samples prepared were then analyzed by means of DSC in order to confirm their glassy character and measure the glass transition temperature. Fig.3.4 shows the DSC spectrum obtained for the samples of the series $x\text{CdI}_2-(100-x) [2\text{Ag}_2\text{O}-(0.7\text{V}_2\text{O}_5-0.3\text{B}_2\text{O}_3)]$ with $x=5, 10, 15, 25$ and 30 . The glass transition temperature T_g is indicated by a base line shift (endothermic) and crystallization of the glass is shown by an exothermic peak. Table 3.1 indicates the glass transition and crystallization temperature values recorded for various compositions of the glass systems studied. It is observed that the glass transition temperature (T_g) decreases with the CdI_2 content. It is commonly accepted that T_g is directly correlated with the strength and number of bonds destroyed within the glass network in order to allow its rearrangement in to a thermodynamically stable phase [4,5]. The same should hold for the glasses considered here. As the amount of CdI_2 increased, the decrease in T_g with the dopant content suggests that a larger number of bonds are destroyed within the glassy network because the Cd^{2+} , after leaving their iodine goes to the interstitial network modifying sites which probably opens the structure in order

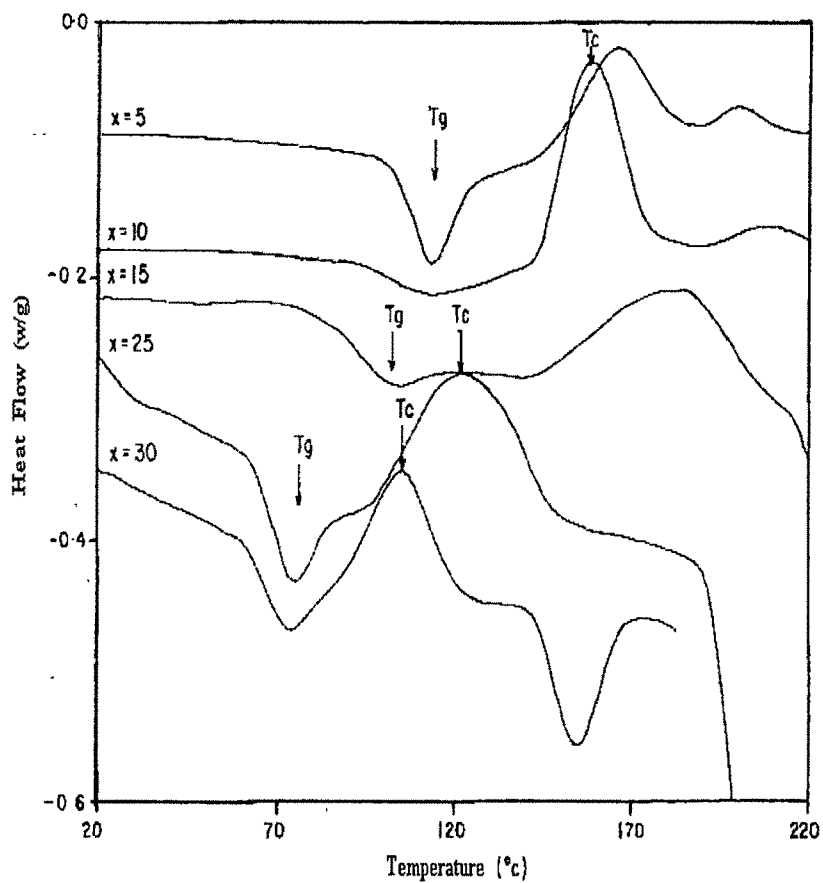


Fig. 3.4. The DSC spectrum obtained for the samples of the series $x\text{CdI}_2-(100-x)[2\text{Ag}_2\text{O}-(0.7\text{V}_2\text{O}_5-0.3\text{B}_2\text{O}_3)]$ with $x=5, 10, 15, 25$ and 30 .

Table 3.1

DSC data of series 1, 2 and 3.

Series 1	$x\text{CdI}_2-(100-x) [2\text{Ag}_2\text{O}-(0.7\text{V}_2\text{O}_5-0.3\text{B}_2\text{O}_3)]$	
CdI_2	T_g	T_c
05	380.3K	438.3K
10	376.0K	431.1K
15	369.1K	457.3K
20	352.5K	425.6K
25	340.6K	394.4K
30	340.5K	377.2K
Series2 (x/y)	$20\text{CdI}_2-80[x\text{Ag}_2\text{O}-y(0.7\text{V}_2\text{O}_5-0.3\text{B}_2\text{O}_3)]$	
1.00	-	373.4K
1.25	336.9K	374.6K
1.50	353.6K	392.3K
1.75	354.0K	398.2K
2.00	352.5K	425.6K
2.25	357.2K	421.8K
2.50	355.6K	424.9K
2.75	354.7K	418.2K
3.00	350.6K	401.8K
Series 3 (x)	$20\text{CdI}_2-53.4\text{Ag}_2\text{O}-26.6[x\text{B}_2\text{O}_3-(1-x)\text{V}_2\text{O}_5]$	
0.0	347.2K	393.6K
0.2	354.3K	430.2K
0.4	356.5K	420.8K
0.6	341.2K	378.5K
0.8	419.6K	533.0K
1.0	424.7K	-

to allow its rearrangement to form a more open type thermodynamically stable phase. Similar decrease in the T_g value with the dopant addition to glass system is seen for many materials [5-7]. At temperatures just below 420K, it is conventional to describe AgI as β -AgI, before it undergoes a transition to the high temperature phase (α -AgI) at 420K. Iodide ions in α -AgI exhibit a bcc arrangement thus help in the Ag^+ ion conduction. The endothermic peak obtained at around 423K for 30 mole% of CdI_2 in the Fig.3.4, ($x=30$), can be attributed to the characteristic β to α phase transition temperature of pure AgI.

Fig.3.5 shows the DSC spectrum obtained for the second series $20CdI_2-80[xAg_2O-y(0.7V_2O_5-0.3B_2O_3)]$ with $x/y = 1.5, 1.75, 2.25, 2.5$ and 3 . An endothermic peak corresponding to glass transition temperature (T_g) has been obtained for all the electrolyte with $x/y > 1$. The DSC results confirmed the x-ray diffraction analysis results, where the electrolyte with $x/y=1$ is found to be polycrystalline. Table 3.1 shows the glass transition temperature and crystallization temperature obtained for the series 2. The T_g value is found to increase till x/y ratio 2.25 and then decrease. This is because T_g depends mainly on the dopant concentration.

Fig.3.6 shows the DSC spectrum obtained for the series 3, $20CdI_2-53.4Ag_2O-26.6[xB_2O_3-(1-x)V_2O_5]$, where $0 \leq x \leq 1$. Table 3.1 shows the glass transition temperature and crystallization temperature value obtained for the series 3. It is found that T_g is almost independent of x . This is because T_g depends mainly on the dopant concentration [8,9] which in this case remains the same. The presence of more than one former increases the units (VO_4 and BO_4) there by decreasing their energy separation. When these separation intervals are small enough, the introduction of the doping salt may induce new distribution of units, and the resulting glass structure shows a different T_g variation

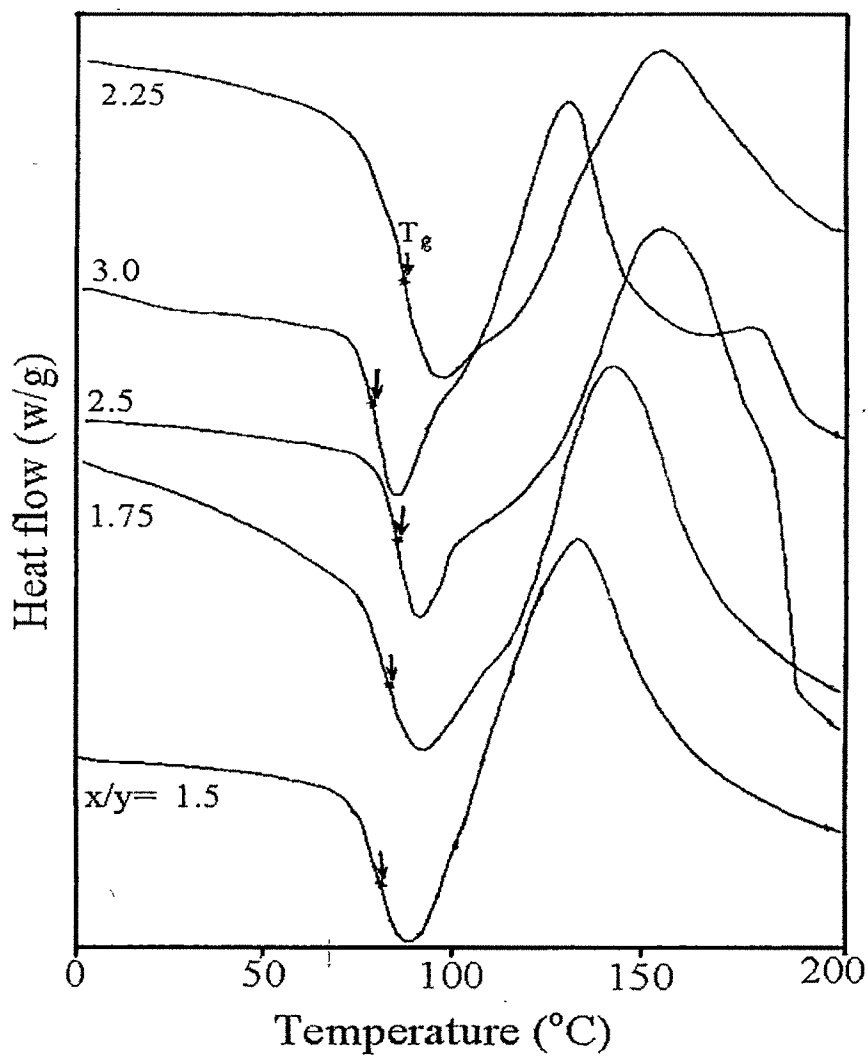


Fig.3.5. The DSC spectrum obtained for the second series $20\text{CdI}_2\text{-}80[\text{xAg}_2\text{O-}y(0.7\text{V}_2\text{O}_5\text{-}0.3\text{B}_2\text{O}_3)]$ with $x/y=1.5, 1.75, 2.25, 2.5$ and 3 .

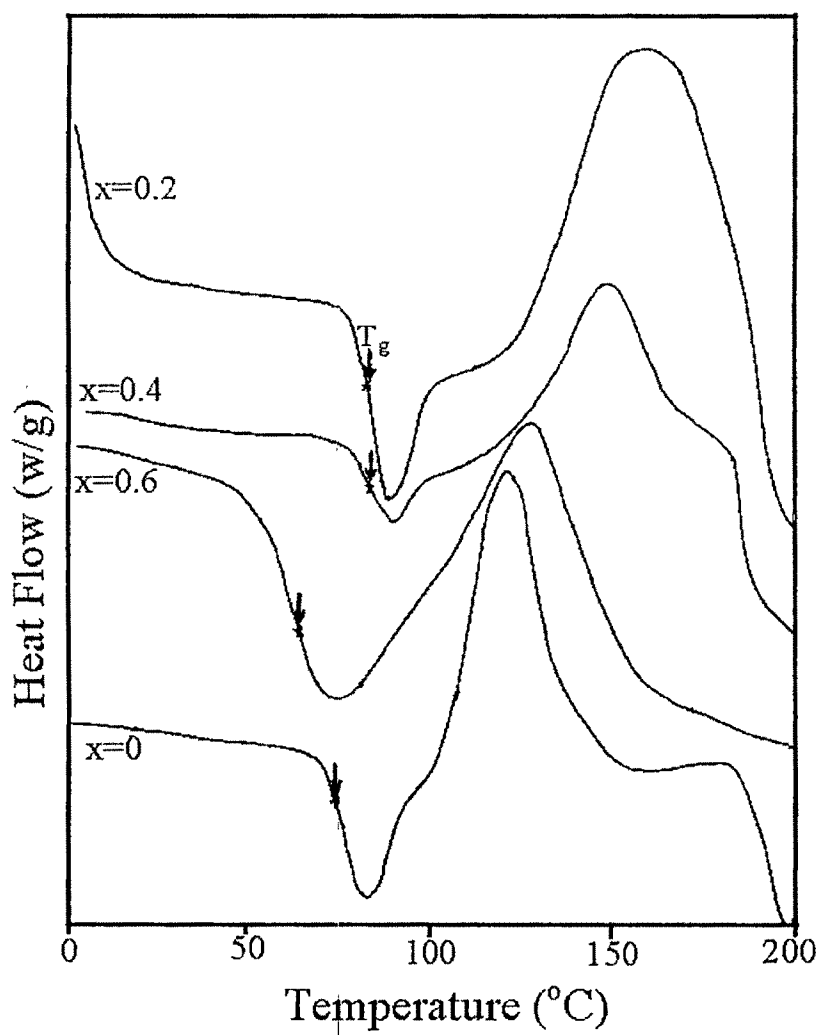


Fig.3.6. The DSC spectrum obtained for the series, $20\text{CdI}_2\text{-}53.4\text{Ag}_2\text{O-}26.6[x\text{B}_2\text{O}_3\text{-(}1\text{-}x)\text{V}_2\text{O}_5]$ for different x values.

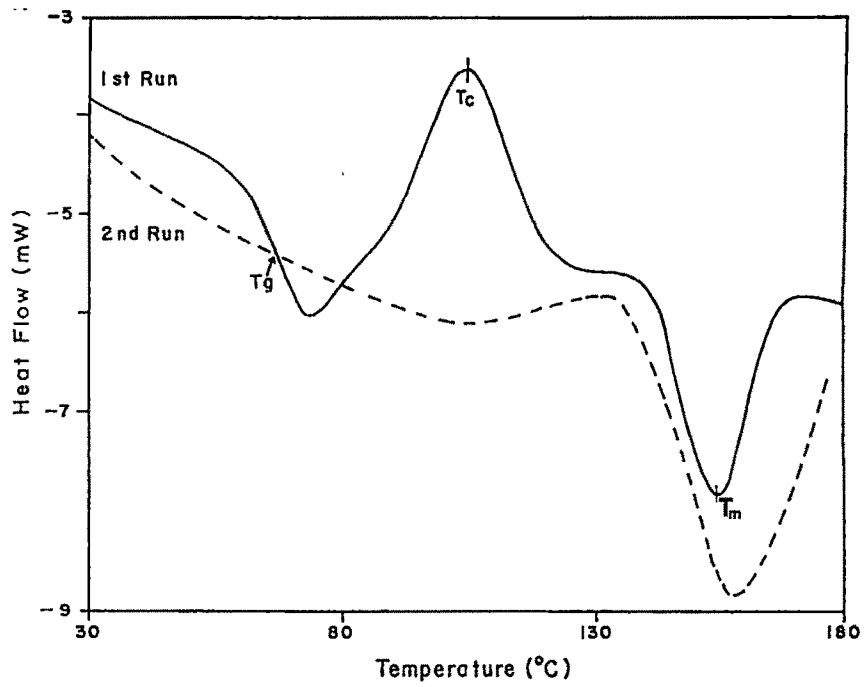


Fig. 3.7. DSC spectrum of the glass material in the first and second run

which may increase, decrease or remain unchanged depending on the former ratios. It is reported [10] for lithium borophosphate glasses that the variation of T_g with different B_2O_3/P_2O_5 ratios does not follow any set of rule. It increases, decreases or remains unchanged depending upon the composition of the mixed network. The glass transition temperature observed for $x=0.8$ and 1 are comparable to the characteristic β - α phase transition temperature of pure AgI ($\sim 420K$) [8]. These results suggest the presence of AgI in these compositions confirming the XRD results discussed earlier.

After the first run, the samples were cooled down to room temperature inside the furnace and then the DSC run were repeated. The second trace did not include either glass transition or crystallization features is shown in Fig.3.7. It is easily understandable that the sample cooled down slowly after the first run, is no longer amorphous but polycrystalline.

3.3. Fourier Transform Infrared Spectroscopy

Infra red spectroscopy is an established analytical technique that identifies compound by finger print light absorption spectra. The most important advantage of infrared spectroscopy is that it provides useful information about the structure of molecule with out any kind of evaluation. A chemical substance shows marked selective absorption of IR radiation, which is due to the changes of vibrational and rotational stages and gives rise to closely packed absorption band called an IR absorption spectrum. Different bands observed in IR spectrum correspond to the characteristic functional groups and bonds found in chemical molecule. Thus, an IR spectrum of a chemical substance is a finger print for its identification.

The term IR covers a range of electromagnetic spectrum between 0.78-1000 μm . In IR spectroscopy, the absorption is expressed in wave number ν , whose unit is cm^{-1} . It is divided into three regions (1) near infra red region spread over from 0.78 μ to 2.5 μ , (2) middle infra red region lies in the range 2.5 μ -15 μ and (3) far infra red region lies between 15 μ -200 μ . The most useful IR region is 2.5 μ -25 μ or 4000 cm^{-1} to 400 cm^{-1} because it gives the important information about the vibration of the molecules and hence its change in structure due to compositional variations [11,12].

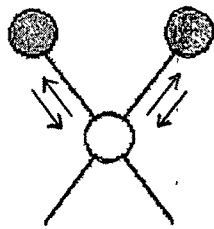
Brief theory of Infrared Spectroscopy

For a molecule to absorb infra red radiation, certain requirement has to be fulfilled. The natural frequency of vibration of the molecule is the same as the frequency of the incident radiation. The vibrations and rotations within the molecule must cause a net change in the dipole moment of the molecule. The alternating electric field of the radiation interacts with fluctuations in the dipole moment of the molecule. If change in the electric field of IR radiation causes a change in the polarity periodically, it means that the spacing between the charged atoms of the molecule also changes periodically and vibration of these charged atoms cause the absorption of IR radiation.

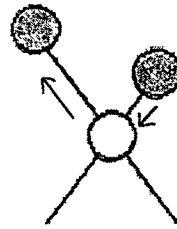
The types of molecular vibrations

The positions of atoms in a molecule is not fixed, they are subjected to a number of different vibrations and rotations. Two atoms are joined by a covalent bond which may undergo stretching vibrations. Three atoms can undergo a variety of stretching and bending vibrations. Energy of a vibration depends on (1) the mass of the atom present in a molecule (2) strength of the bond (3) the arrangement of various atoms in a molecule.

Stretching vibrations: It arises due to stretching and contracting of bond with out



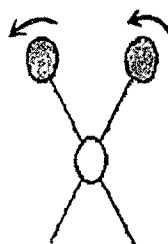
Symmetric



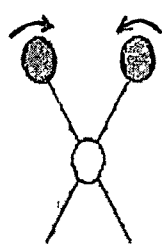
Asymmetric

Stretching Vibrations

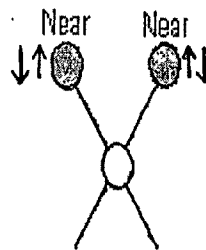
(a)



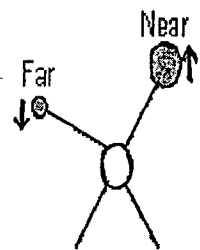
In-plane rocking



In-plane scissoring



Out-of-plane wagging



Out-of-plane twisting

Bending Vibrations

(b)

Fig.3.8 (a) Stretching and (b) bending vibration of the molecule

producing any change in the bond angles, which are of two types, in Fig.3.8 (a).

- (1) **Symmetric stretching:** The movement of atoms with respect to a particular atom in a molecule is in the same direction.
- (2) **Asymmetric stretching:** If one atom approaches the central atom whereas the other approaches away from it in a triatomic system. Because of this the change in electric dipole takes place. Therefore asymmetric stretching gives it vibrational frequency at higher wave number than for symmetric system.

Bending vibrations: It gives rise to deformation of bond angle but there is no change in bond lengths which are classified into four types, in Fig.3.8 (b).

- (1) **Scissoring:** The two atoms approach each other in the same plane.
- (2) **Rocking:** The movement of atoms occurs in the same direction and also in the same plane.
- (3) **Wagging:** The two atoms move up and down below the plane with respect to the central atom.
- (4) **Twisting:** One of the atoms moves up the plane and the other moves down the plane with respect to the central atom.

The energy required to stretch a spring is more than that needed to bend it so the stretching absorption of the bond will appear at higher frequencies than the bending absorption of a bond. Thus, IR spectroscopy is widely used for molecular structural studies of various glasses.

In glasses, the bands are generally broader and overlapping than those observed in crystalline materials. This is because of the lack of long range order in glasses and is similar to the broadening of the spectra observed in other techniques [13-16].

The IR spectra are recorded for all the samples of the three series to understand the type of vanadoborate structural units, the effect of the dopants and any change due to the variation of modifier and glass formers. The changes in molecular structure, bond length and vibrational group have been studied with IR spectroscopy.

Fig.3.9 shows the FTIR spectra of pure B_2O_3 and V_2O_5 which are taken for the purpose of comparison. The spectra for pure B_2O_3 show the characteristic absorption band at 1471cm^{-1} , 1200cm^{-1} , 820cm^{-1} and 550cm^{-1} . The peak at 1471cm^{-1} and 1200cm^{-1} are assigned to BO_3 triangle [17-19]. The peak at 820cm^{-1} and 550cm^{-1} are attributed to bending vibrations of B-O-B bond [15,20,21]. The B_2O_3 structure consists of BO_3 triangles, which are randomly oriented in the three dimensional network [15, 19].

The FTIR spectra of pure V_2O_5 which has characteristic features at 1020cm^{-1} , 840cm^{-1} and 613cm^{-1} . The V_2O_5 structure is built up by deformed VO_5 trigonals bonded in zigzag chains. Each VO_5 group contains a short V=O bond (vanadyl group) [22, 23]. The sharp band at 1020cm^{-1} is assigned to the vanadyl group of V=O bond. The broad band observed at 840cm^{-1} is attributed to the asymmetric vibrations along the V-O-V bonds involved in the corner sharing of VO_5 polyhedra [24]. A weak absorption peak present 613cm^{-1} corresponds to V-O-V bond of symmetrical or bending mode of vibration [15].

In the first series, the amount of dopant is increasing from 5 to 30 mole% whereas the glass modifier to former ratio is kept in the ratio 2:1. The FTIR spectra of all the samples of first series are shown in Fig.3.10. In this series the band position obtained are not changing for different dopant composition. The infra red absorption spectrum shows

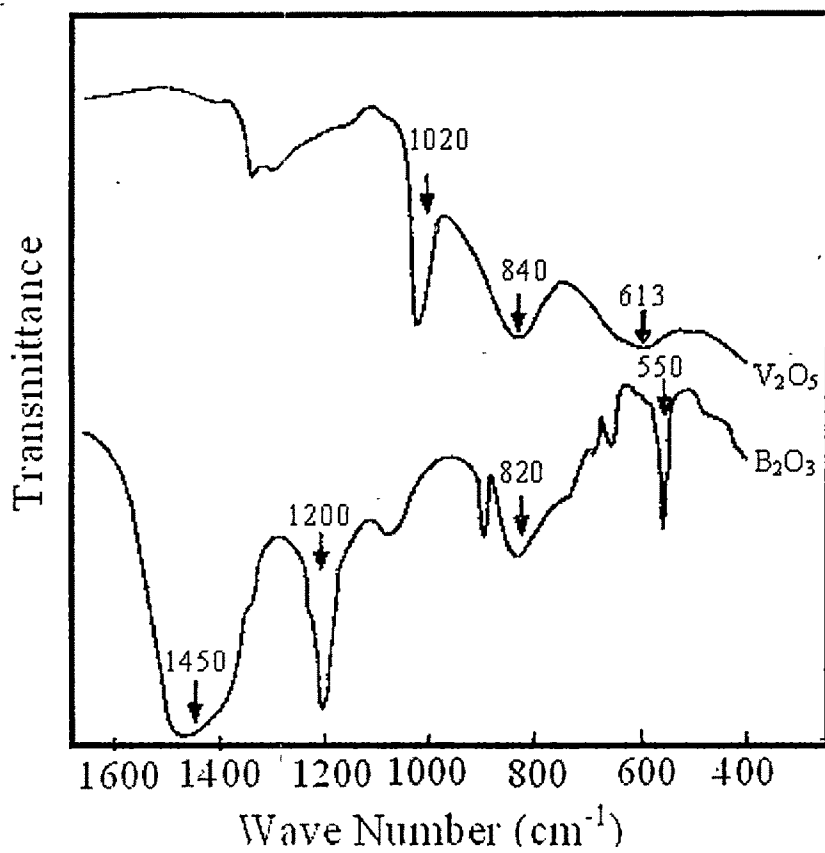


Fig.3.9 IR spectra of crystalline V₂O₅ and B₂O₃

different bands at 500 cm^{-1} , 714 cm^{-1} , 855 cm^{-1} , 894 cm^{-1} , 923 cm^{-1} , 966 cm^{-1} , 1008 cm^{-1} , 1438 cm^{-1} .

Anderson et. al., [25] suggest that the spectrum of pure borate glasses is consisted of BO_3 triangles randomly oriented sharing corners with each oxygen shared by two borons. The spectrum of fused B_2O_3 not only is consisted of a completely continuous triangle like network but also contains some BO_4 tetrahedra. It is suggested that [25] the absorption peak at 1460 cm^{-1} , 1200 cm^{-1} and 780 cm^{-1} are related to BO_3 triangles. The weaker peaks at 1115 cm^{-1} , 1030 cm^{-1} , 930 cm^{-1} and 740 cm^{-1} are assigned to BO_4 tetrahedra. The band at 1220 to 1400 cm^{-1} [25] are characteristic of $=\text{B}-\text{O}-\text{B}\equiv$ linkage in which one of the boron is tetrahedrally coordinated and those at 1333 to 1428 cm^{-1} show the presence of tetrahedrally coordinated boron in the structure. Jelly and Proctor [26] have shown that the 690 to 714 cm^{-1} band is triangularly coordinated borate groups. Kulieva et. al., [19] suggest that the band at 1020 cm^{-1} and 820 cm^{-1} are due to the stretching vibrations of $\text{V}=\text{O}$ bonds and the band between 400 - 700 cm^{-1} are due to the asymmetric and symmetric stretching vibrations of $\text{V}-\text{O}-\text{V}$ respectively.

The band reported here at 500 cm^{-1} , 714 cm^{-1} , 855 cm^{-1} , 894 cm^{-1} , 923 cm^{-1} , 966 cm^{-1} would seem to be attributable to the vanadate phase. The band observed at 923 cm^{-1} results from the vibration of the independent $\text{V}=\text{O}$ bond in the VO_5 groups whereas in pure V_2O_5 , it is seen at 1020 cm^{-1} . The displacement of frequency towards the lower wave number is the proof for the interaction of Ag^+ ion with $\text{V}=\text{O}$ bonds and the transformation of VO_5 groups into VO_4 groups [23]. It is due to the fact that the added Ag_2O goes into the structure at interstitial positions leaving its oxygen. Some of the Ag^+ ions now interact directly with the oxygen of the $\text{V}=\text{O}$ bond, which are thereby weakened

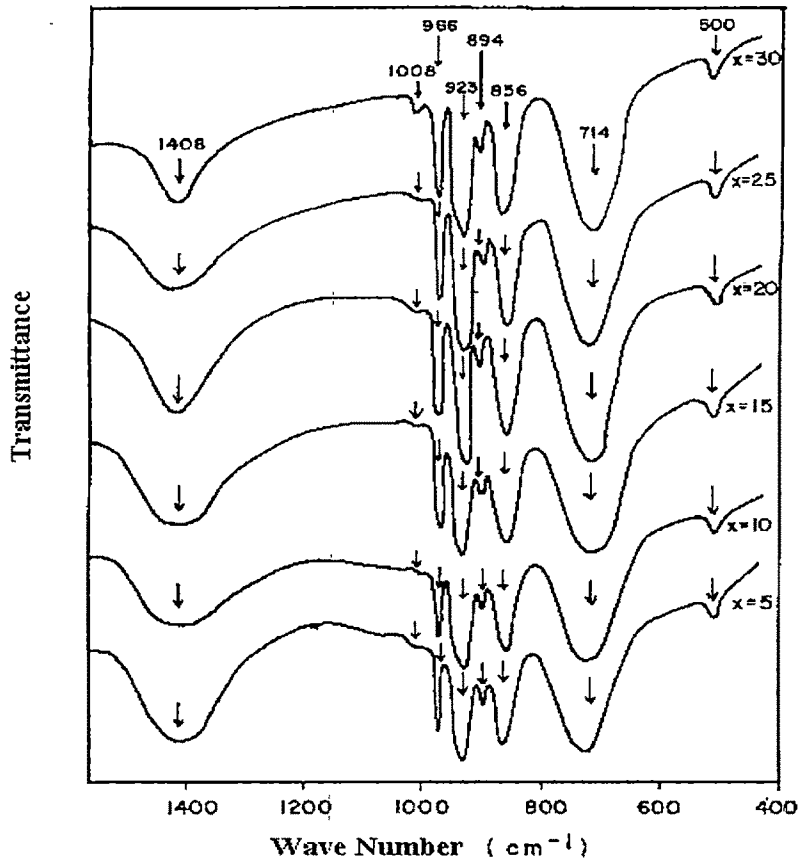


Fig.3.10. FTIR spectra for the system $x\text{CdI}_2-(100-x)[2\text{Ag}_2\text{O}-(0.7\text{V}_2\text{O}_5-0.3\text{B}_2\text{O}_3)]$, where $x=5,10,15,20,25,30$

and the frequency of vibration shifts towards the lower wave number. The added Ag_2O also gives rise to the formation of non-bridging oxygens, there by creating VO^- unit [20]. It is obvious that the oxygen, which becomes non-bridging and acquires a negative charge, will move closer to the connected vanadium, consequently reducing the positive charge on the vanadium ions and there by resulting in a decrease in the binding of other oxygens attached to this particular ion, therefore the length of the $\text{V}=\text{O}$ increases. This elongation of the $\text{V}=\text{O}$ bond leads to the shift of frequency to 923cm^{-1} as seen from the spectrum [27]. The band observed at 966 cm^{-1} is assigned to the symmetric stretching vibration of VO_2 groups in the VO_4 polyhedra [28]. The band at 894 cm^{-1} is assigned to the asymmetric vibration of the V-O-V bond involved in the corner sharing of VO_5 polyhedra where as the band at 500 cm^{-1} (ν_{sym}) and at 714 cm^{-1} (ν_{asym}) are assigned to V-O-V bridge stretching [3]. The 714 cm^{-1} band observed here may either be due to the B-O-B linkage also in which both the borons are triangularly coordinated [29]. A weak band observed at 1008 cm^{-1} is due to the presence of BO_4 groups. The absorption peak observed at 1438 cm^{-1} is assigned to the vibration of the boroxol ring. The band observed at 855 cm^{-1} represents B-O stretching vibration of $(\text{BO}_4)^{5-}$ units. Infra red absorption spectra indicate that the vibrational frequencies of the vanadoborate network are not affected by the incorporation of the doping salt CdI_2 . The above IR spectra of different dopant concentration are quite similar to other well known AgI doped Ag oxysalt glassy systems [3.5.29.30].

In the second series, $20\text{CdI}_2\text{-}80[\text{xAg}_2\text{O-y}(0.7\text{V}_2\text{O}_5\text{-}0.3\text{B}_2\text{O}_3)]$, the amount of dopant is fixed and modifier to former ratio is increasing from 1 to 3 in steps of 0.25. The FTIR spectrum obtained for all the samples is shown in Fig.3.11. The infra red absorption

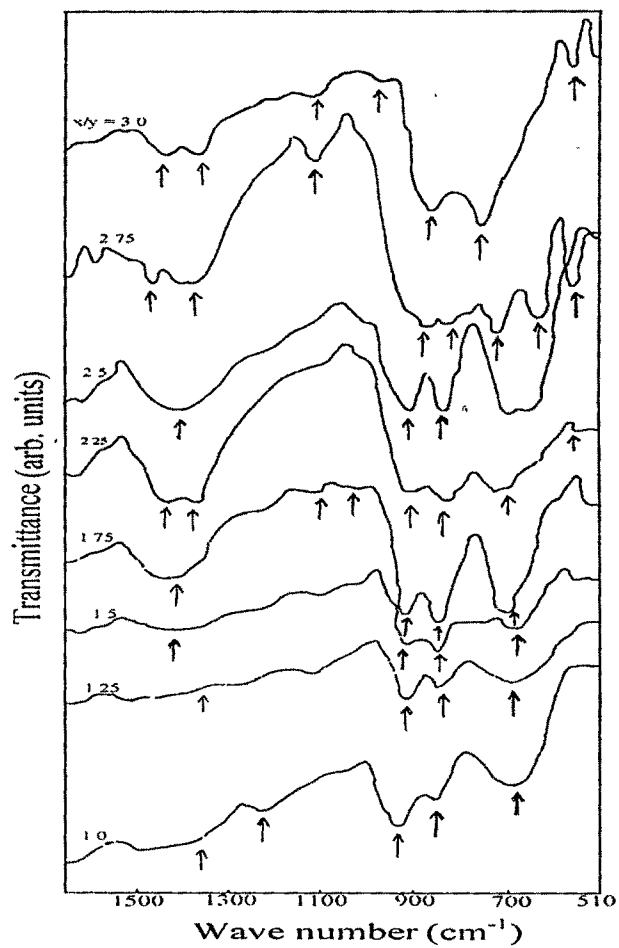


Fig.3.11. FTIR Spectra for the system $20\text{CdI}_2-80[x\text{Ag}_2\text{O}-y(0.7\text{V}_2\text{O}_5-0.3\text{B}_2\text{O}_3)]$ with different x/y ratios.

spectrum shows different bands at 1460cm^{-1} , 1399cm^{-1} , 1205cm^{-1} , 1134cm^{-1} , 1029cm^{-1} , 923cm^{-1} , 893cm^{-1} , 854cm^{-1} , 711cm^{-1} and 564cm^{-1} .

The absorption peak observed in the present series at $1460\text{-}1412\text{cm}^{-1}$ is assigned to the vibration of the boroxol ring. As the amount of modifier increases, there is a shift in the vibration band towards lower wave number and is ascribed to the increase in the bond length of B-O groups and the formation of BO_4 units. The incorporation of modifier (Ag_2O) to the glass former matrix gives an extra oxygen atom which is accommodated in the network leads to the transfer of some boron atoms from triangle BO_3 to BO_4 [9]. In pure borate glasses, the main structural element is the boroxol ring of plane, trigonal configuration with a B-O bond length $1.36\pm 0.005\text{\AA}$, whereas as, the B-O bond length for BO_4 tetrahedra was observed to be $1.47\pm 0.01\text{\AA}$. In IR spectra, the increase in bond length is seen as a shifting of an absorption band towards lower wave number. One modifier causes the formation of two BO_4 tetrahedra, which participate in the three dimensional network, thus strengthening the structure [31].

As the modifier to former ratio increases, the vibrational band at 1460cm^{-1} split into two vibrations 1446cm^{-1} and 1376cm^{-1} which are assigned to the characteristics of B-O-B linkage in which both the borons are triangularly coordinated. The weak absorption band observed at 1205cm^{-1} can be assigned to the B-O stretching of the BO_3 group with a non-bridging oxygen atom. A weak vibrational peak observed at 1134cm^{-1} is assigned to the vibrations of non-bridging oxygen in the form $>\text{B-O}^-$ or $\text{B-O-B}<\text{O}^-$. For the system with $x/y=1.75$, a new weak absorption peak is observed at 1029cm^{-1} which is assigned to the vibration of BO_4 groups. The band observed at 855cm^{-1} represents B-O stretching vibrations of $(\text{BO}_4)^{5-}$ units or of the V-O-V stretching vibrations. The

absorption band observed at 923 cm^{-1} is assigned to the isolated V=O which is a shift in the vibrational band towards the lower wave number, suggests the increase in the bond length of isolated V=O bond. The 714 cm^{-1} band observed here may either be due to the V-O-V bridge stretching vibrations. With the increasing addition of Ag_2O another small band at 585 cm^{-1} is due to the symmetric vibration of V-O-V bond. From this it is clear that the modifier Ag_2O is responsible for bringing changes in the vibrational bands related to borate and vanadate group in the present series.

Similarly in the third series, $20\text{CdI}_2\text{-}56.4\text{Ag}_2\text{O}\text{-}26.6[x\text{B}_2\text{O}_3(1-x)\text{V}_2\text{O}_5]$, where $x=0$ to 1 in steps of 0.2, the IR spectra has been taken to understand the effect of glass formers. Here the amount of dopant and the glass modifier is constant and one of the glass former (V_2O_5) is replaced by another (B_2O_3). Fig.3.12 shows the FTIR spectra of the samples of series 3. The spectra shows the absorption bands at 1443cm^{-1} , 1376 cm^{-1} , 1243 cm^{-1} , 1113 cm^{-1} , 1010 cm^{-1} , 926 cm^{-1} , 853 cm^{-1} , 714 cm^{-1} , 657 cm^{-1} , 591 cm^{-1} .

In the first sample, where $x=0$, the peaks at 1443cm^{-1} , 1376 cm^{-1} , 1243 cm^{-1} and 1113 cm^{-1} are not observed which is a clear indication of the absence of B_2O_3 in the system. With the increasing addition of B_2O_3 , 1443cm^{-1} , 1376 cm^{-1} , 1243 cm^{-1} and 1113 cm^{-1} peaks appear and shift towards the lower frequencies. The increased addition of B_2O_3 shows the peaks at 1243cm^{-1} and 1010cm^{-1} and is due to the B-O vibration of BO_3 and the BO_4 groups. The peak observed at 1113cm^{-1} is assigned to the vibrations of non-bridging oxygen in the form $>\text{B-O}^-$ or $\text{B-O-B}<\text{O}^-$. As the mole % of B_2O_3 increases at $x=0.6$, 0.8 and 1 the vibrational band at 653cm^{-1} is observed and is due to the bending vibration of the B-O-B bond. The extra peak observed with the increasing addition of B_2O_3 shows the effect of Ag_2O in the B_2O_3 network. The band observed at 853cm^{-1} is

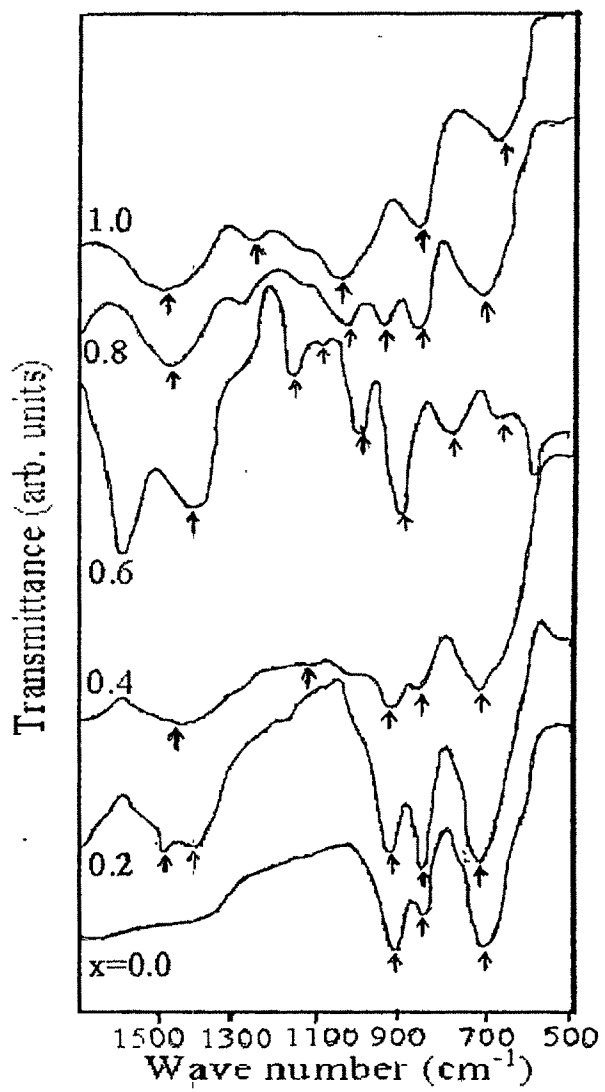


Fig.3.12. FTIR spectra for the system $20\text{CdI}_2\text{-}56.4\text{Ag}_2\text{O-}26.6 [x\text{B}_2\text{O}_3\text{-(}1\text{-}x\text{)V}_2\text{O}_5]$, with different x values.

assigned to either BO_4 groups or V-O-V bridge stretching. The sample with $x=0.8$ and 1 do not show the absorption band at 714cm^{-1} which is due to the asymmetric vibration of the V-O-V bridge stretching and $x=1$ sample shows the absence of 923cm^{-1} peak which is assigned to the vibration of the independent V=O bond in the VO_5 groups. The shifting of the band position is seen from $714\text{-}777\text{cm}^{-1}$ as the amount of B_2O_3 increases. A small peak at 591 cm^{-1} for $x=0.6$ indicates the presence of V-O-V vibration. The absence of 714cm^{-1} and 923cm^{-1} peak in the sample with $x=1$ shows the absence of V_2O_5 in this system.

3.4. Density measurements

Density of a glass is explained in terms of masses and sizes of the various structural groups present in glass. Accordingly, density is related to how tightly the ions and ionic groups are packed together in the sub-structure. Density measurements for all the samples were determined using Archimedes method. Molar volume, ion concentration, inter ionic spacing have been calculated by knowing the density and chemical composition of the glass samples. Table. 3.2 shows the density, molar volume, Ag^+ and I^- ion concentration, Ag-Ag spacing and Ag-I spacing for the three series. For the first and second series, the density of the material increases with the dopant addition and the increase of the modifier content. For the third series the value obtained is almost constant. In the first series, with the addition of dopant the molar volume increases, which shows the structure of the system expands with the addition of CdI_2 . Similar increase in molar volume with PbI_2 doped $\text{Ag}_2\text{O-V}_2\text{O}_5$ systems has been reported [3]. The increase in the conductivity of the first series (discussed in next chapter) with the addition of dopant is due to the formation

Table 3.2

Density, Molar volume, Ag^+ and I^- ion concentration, Ag-Ag and Ag-I spacing of the three series studied.

Series	Mole%	Density (gm/cc)	Molar Volume $\times 10^{21}$ moles	ion concentration (mole/cm ³)		Ag-Ag spacing $\times 10^{-8}$ cm	Ag-I spacing $\times 10^{-8}$ cm
				Ag^+ $\times 10^{-2}$	I^- $\times 10^{-3}$		
Series 1	x= 5%	5.346	1.482	3.11	2.46	3.760	8.769
	10	5.442	2.913	2.89	4.82	3.853	7.001
	15	5.632	4.369	2.74	7.25	3.926	6.116
	20	5.712	5.755	2.65	9.55	4.022	5.755
	25	5.804	7.032	2.33	11.6	4.142	5.219
	30	5.966	8.409	2.17	13.9	4.243	4.917
Series 2	x/y=1%	5.571	5.792	1.92	9.61	4.419	5.568
	1.25	5.629	5.777	2.13	9.59	4.268	5.574
	1.50	5.686	5.778	2.30	9.58	4.162	5.573
	1.75	5.704	5.798	2.45	9.62	4.076	5.566
	2.00	5.712	5.755	2.53	9.49	4.022	5.593
	2.25	5.733	5.706	2.62	9.47	4.031	5.596
	2.50	5.804	5.747	2.73	9.54	3.985	5.582
	2.75	5.881	5.799	2.83	9.62	3.923	5.566
3.00	5.933	5.830	2.90	9.67	3.852	5.556	
Series 3	x=0%	5.351	5.253	2.32	8.72	4.146	5.752
	0.2	5.551	5.519	2.44	9.16	4.078	5.658
	0.4	5.697	5.738	2.54	9.53	4.026	5.585
	0.6	5.823	5.942	2.63	9.87	3.979	5.521
	0.8	5.948	6.151	2.72	10.2	3.900	5.400
	1.0	5.859	6.139	2.72	10.2	3.900	5.462

of AgI in this system and their mobility. The Ag^+ ions attached to the I ions are less tightly bound than those Ag^+ ions with the vanadoborate matrix. The conductivity depends on the mobile ion concentration and their mobility. The concentration of the mobile ions is found to increase with the increase in the dopant addition due to the increase in the formation of AgI clusters. The mobility of these ions may also increase because of the increase in the molar volume [32]. Table 3.2 shows the Ag^+ ion concentration is found to decrease in the first series with the addition of dopant and in the second series it is found to increase with the increase in the modifier to former ratio. The Ag-Ag spacing is found to increase in the first series while the Ag-I spacing is found to decrease. In the second series Ag-Ag spacing is found to decrease with the x/y ratio while the Ag-I spacing is found to decrease up to x/y ratio 1.75 and then increases up to 2.25 and then again decreases. The variation in this Ag-I spacing is similar to the conductivity variation (chapter 4) found in the second series. In the third series Ag-Ag distance is found to decrease and the Ag-I distance is found to decrease up to $x=0.8$ and then slightly increases for the last sample.

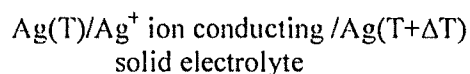
3.5. Thermo electric Power

When a temperature gradient exists in a solid containing lattice defects owing to the increased concentration and increasing jump frequency of the defects near hot end, a flow of defects from hot to cold region is set up. At steady state, a voltage across the sample appears and the hotter end become positive or negative depending on the sign of the moving charges. In fast ion conductors based on AgI, Ag^+ ions are the charge carriers making the hotter end negative, thus it reflects the sign of the charge carriers in the system.

Thus the thermo electric power (TEP) measurement is the most powerful tool for examining the nature of the charge carriers in any system.

Thermo electric power studies provide further insight into understanding the ion transport mechanisms in high conducting systems. Thermo electric power measurements have many advantages based on the fact that it is a zero current process. These measurements will not modify the equilibrium distribution of ions provided they are carried out properly with small thermal gradients. In the case of poly crystalline materials, the grain boundary between particles causing contact resistance and capacitive effect do not affect the TEP since the impedance offered by them towards the heat flow is negligible [33]. Contact problems are also reduced by the zero current nature of the TEP measurements. TEP studies on Ag based fast ion conductors are simpler than other conventional ionic solids due to the fact that in silver ion conductors, the transport mechanism is fairly simple and the concentration of mobile charge carriers is large and almost constant with temperature, and is reported in the literature by many authors [34 - 40]. These are electronic insulators. In silver ion conductors one can conveniently use reversible Ag electrodes where as in alkali halides, none of the alkali metals or halogens could be conveniently used as electrodes [33].

In the present investigation, the thermo cell used was of the following configuration



It is well known that TEP consists of two parts (1) the homogeneous TEP θ_{hom} arising due to the temperature gradient across the sample and (2) heterogeneous TEP θ_{het} resulting due to temperature variation of electrode-electrolyte contact potential. Thus,

$$\theta = \theta_{\text{hom}} + \theta_{\text{het}} \quad (3.4)$$

For the case of usual ionic solids (alkali or silver halides) the expression for θ_{hom} due to several workers [33-35] is given by the following equation

$$\theta_{\text{hom}} = - \sum_1^n \left[\frac{t_r (\text{grad} \mu_r) T}{e_r \text{grad} T} + \frac{t_r q_r^*}{e_r T} \right] \quad (3.5)$$

t_r is the transport number, μ_r the chemical potential, q_r^* the heat of transport and e_r the charge on the species r . Subscript r in each case denote the type of charge carrying species. In the case of materials of the system studied here $\text{CdI}_2\text{-Ag}_2\text{O-V}_2\text{O}_5\text{-B}_2\text{O}_3$ it is confirmed that the formation of AgI in this system and the Ag^+ ion from this AgI help in conduction. Then the subscript r may be replaced by Ag^+ in Eqn.3.5 and that the transport number of Ag^+ ion t_{Ag^+} is found to be unity. In view of these facts the expression for θ_{hom} for the presently studied materials (pure cationic conductors) reduces to

$$\theta_{\text{hom}} = - \frac{(\text{grad} \mu_{\text{Ag}^+}) T}{e \text{grad} T} - \frac{q_{\text{Ag}^+}^*}{e T} \quad (3.6)$$

where e is the electronic charge. For an ionic solid in contact with its cationic metal (say salt MX in contact with M) θ_{het} have been evaluated by several authors which for the case of our solid in contact with silver may be written as

$$\theta_{\text{het}} = \frac{1}{e} \frac{\partial \mu_{\text{Ag}^+}}{\partial t} + \frac{1}{e} S_{\text{Ag}^+}^{\text{Ag}} \quad (3.7)$$

where $S_{\text{Ag}^+}^{\text{Ag}}$ is the partial entropy of Ag^+ ion in silver metal. The chemical potential of Ag^+ ion is related with its number n_{Ag^+} per unit volume by the relation.

$$\mu_{\text{Ag}^+} = g_{\text{Ag}^+} + kT \ln \frac{n_{\text{Ag}^+}}{N} \quad (3.8)$$

where N is the number of normal sites per unit volume, g_{Ag^+} is the amount of work required to bring an Ag^+ ion from a state of rest at infinity to an interstitial position in the solid at constant temperature and pressure. Using Eqn.3.8, the expression for θ_{hom} and θ_{het} given by Eqn. 3.5 and 3.7 reduces to

$$\theta_{hom} = -\frac{kT(gradn_{Ag^+})T}{en_{Ag^+}gradT} - \frac{q_{Ag^+}^*}{eT} \quad (3.9)$$

$$\theta_{het} = \frac{kT(gradn_{Ag^+})T}{en_{Ag^+}gradT} + H \quad (3.10)$$

$$\text{where } H = \frac{1}{e} \left[-S_{Ag^+} + k \ln \frac{n_{Ag^+}}{N} + S_{Ag^+}^{Ag} \right] \quad (3.11)$$

$$-S_{Ag^+} = \frac{\partial g_{Ag^+}}{\partial T} \quad (3.12)$$

A combination of θ_{hom} and θ_{het} gives the following expression for total thermoelectric power

$$\theta = \theta_{hom} + \theta_{het} = -\frac{q_{Ag^+}^*}{eT} + H \quad (3.13)$$

The electrolyte of present study is a sort of cationically disordered solid. In such electrolytes, the number of available sites for Ag^+ ion is much more than available Ag^+ ions. The charge carriers in these solids are not thermally generated but remain almost constant with temperature. The small increase in conductivity with temperature comes due to the increase in the mobility with temperature [43]. Thus the term $k \ln(n_{Ag^+}/N)$ in the expression of H is nearly temperature independent. Also, first and third terms are small and their variation with temperature shall cancel in the expression. In view of these facts, the term H in the expression of θ for pure cationic conductors and with cationically

disordered structure will be almost temperature independent. Thus the θ in these solids should vary linearly with $1/T$ (deg^{-1}) and the slope will be equal to $q_{t,Ag^+}^* / e$ [33].

The thermo emf values observed during the TEP studies for all the samples of the present study are found to be negative when the hot end is connected to the positive polarity of the voltmeter. This means that TEP (θ) values are negative for all the samples thus indicating the charge on the mobile species are positive. Fig.3.13 shows the variation of thermo electric power ($-\theta$) versus $10^3/T$ for the system $x\text{CdI}_2 - (100-x) [2 \text{Ag}_2\text{O} - (0.7\text{V}_2\text{O}_5 - 0.3\text{B}_2\text{O}_3)]$ with different x values. The heat of transport (q_{t,Ag^+}^*) of the mobile species obtained from the slopes of these curves are shown in Table 3.3. The activation energy for Ag^+ ion migration (calculated from the conductivity studies) with the heat of transport estimated from the thermoelectric power study is comparable. The heat of transport which is equal to the static barrier height for ion hopping [35] is, therefore, expected to approach the activation energy of Ag^+ ion migration. Fig. 3.15 and 3.16 shows the thermo electric power plot obtained for series 2 and series 3.

As described earlier, the numbers of sites available for Ag^+ ions are much more than their own number n_{Ag^+} and thus Ag^+ ions are evidently able to jump to a position of equal energy. The distinction between interstitial Ag^+ ions and lattice Ag^+ ions are lost. Thus unlike alkali halides, there is nothing like heat of formation of defects in these electrolytes and hence the heat of transport in such solids may be expected to be close to their activation energies. This conclusion is also justified according to the theory of Rice and Roth which predicts that the two entities should be the same in fast ion conductors. Rice and Roth [41] evolved a model, which allows the theoretical estimation of activation energy and thermo electric power. Their formula is based on the assumption that for

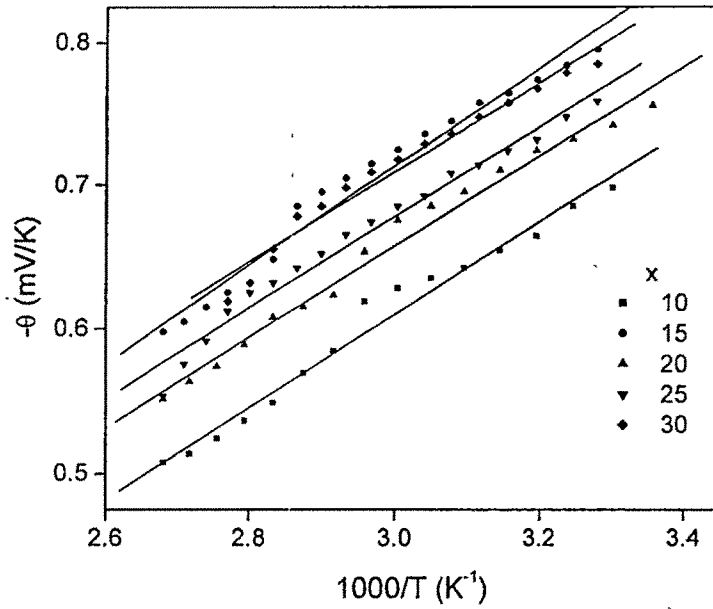


Fig. 3.14 The variation of thermo electric power with inverse of temperature for the system $x\text{CdI}_2-(100-x)[2\text{Ag}_2\text{O}-(0.7\text{V}_2\text{O}_5-0.3\text{B}_2\text{O}_3)]$

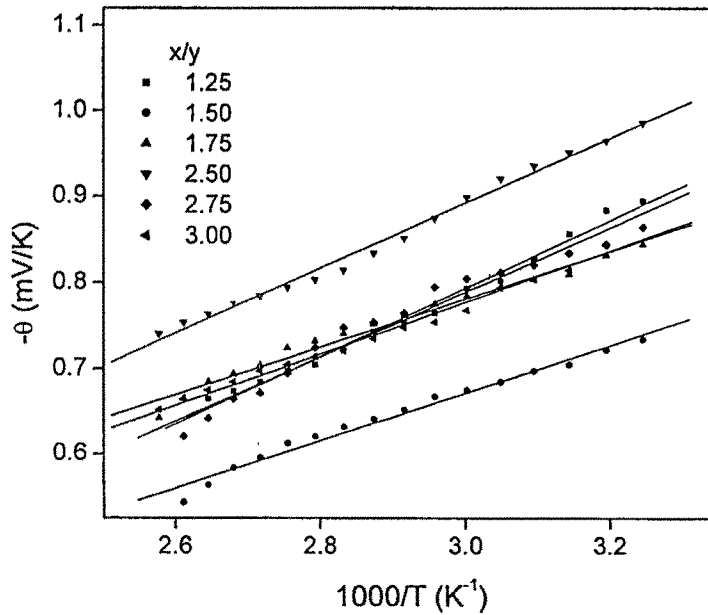


Fig. 3.15. Thermoelectric power plot obtained for the series, $20\text{CdI}_2-80[x\text{Ag}_2\text{O}-y(0.7\text{V}_2\text{O}_5-0.3\text{B}_2\text{O}_3)]$ with different x/y ratios.

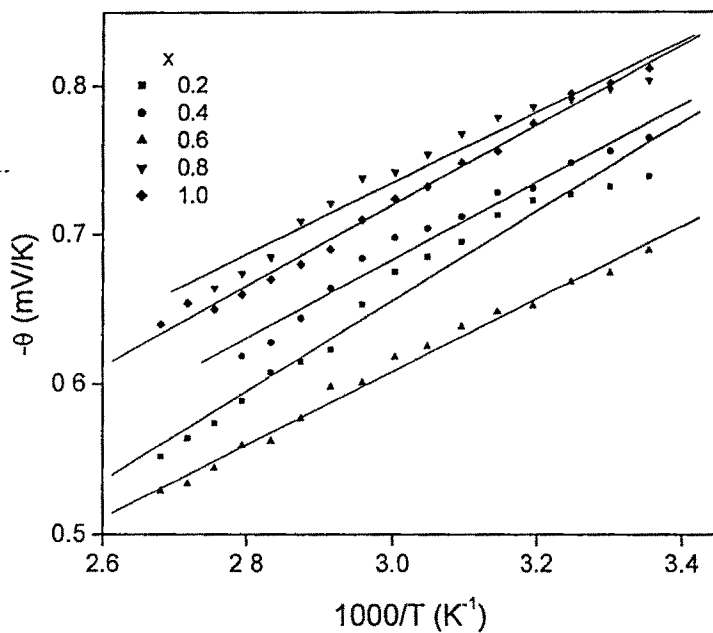


Fig.3.16. Thermoelectric power versus inverse of temperature for the series, $20\text{CdI}_2\text{-}56.4\text{Ag}_2\text{O-}26.6[x\text{B}_2\text{O}_3(1-x)\text{V}_2\text{O}_5]$.

highly disordered solids, the ions in them may be considered to be in the free ion like state.

On the basis of this assumption, they have shown that

$$-\theta_{\text{hom}} = \frac{\Delta h}{eT} \quad (3.14)$$

Δh is the activation energy of mobile ions and

$$-\theta_{\text{hom}} = \frac{q_{\text{Ag}^+}}{eT} \quad (3.15)$$

where q_{Ag^+} is the heat of transport of Ag^+ ions in the material.

$$\Delta h = q_{\text{Ag}^+} \quad (3.16)$$

Eqn.3.16 leads to the conclusion that in the case of highly disordered solids, the ionic heat of transport tends to be equal to its activation energy. Thus, the present model leads us to believe that our electrolyte samples are highly disordered, which is also confirmed through the x-ray analysis. Thus, our results are in accordance with the theory of Rice and Roth [41-43].

3.6. Ionic transport number

Polarization measurements have been used in order to deduce the partial conductivities of the ionic and electronic charge carriers in a conductor. There are essentially two basic analyses which are currently being used. One has been derived by Wagner [44,45] and the other by Danforth and Bodine [46]. In Wagner's method, the mixed conductor MX is placed between a virtually reversible electrode, M, and an irreversible inert electrode, e.g., graphite or platinum as M/MX/inert electrode. A dc potential below the decomposition potential of MX is applied to the cell with the negative pole on the left electrode M of the

cell, the ionic conduction will be suppressed and the resultant current can be used to determine the electronic conductivity in MX [47-49].

3.6.1. Wagner's Polarization technique

The ionic transport numbers (t_{ion}) of the samples were measured by the Wagner's dc polarization method. The ionic transport number (t_{ion}) and electronic transport number (t_e) of the sample were determined by using the relation

$$t_{ion} = I_{ion} / I_T, \quad t_e = I_e / I_T \quad (3.17)$$

where I_{ion} is the current due to the mobile ions, I_e is the electron current and I_T is the total current due to all the mobile species, i.e., ions and electrons.

$$I_T = I_{ion} + I_e \quad (3.18)$$

Fig.3.17 shows the current versus time plot obtained for the series $x\text{CdI}_2-(100-x) [2\text{Ag}_2\text{O}-(0.7\text{V}_2\text{O}_5-0.3\text{B}_2\text{O}_3)]$ with $x=15$ mole % of CdI_2 composition by the Wagner's Polarization Technique. It shows the initial total current (I_T) which is nearly 1.43×10^{-5} A, decreases with time due to the depletion of the ionic species in the electrolyte and becomes constant in the fully depleted situation. At this stage the residual current is only the electronic current (I_e), $\sim 4.8 \times 10^{-7}$ A after 23 hours. The current due to the mobile ion is given by

$$I_{ion} = I_T - I_e \quad (3.19)$$

Therefore the ionic transport number,

$$t_{ion} = 1 - I_e / I_T \quad (3.20)$$

The ionic transport number and electronic transport number calculated for 15 mol% of CdI_2 composition are observed to be 0.9664 and 0.0336 respectively. Fig.3.18 shows the current versus time plot for the series $20\text{CdI}_2-80[x\text{Ag}_2\text{O}-y(0.7\text{V}_2\text{O}_5-0.3\text{B}_2\text{O}_3)]$ with $x/y = 1.5$ and the ionic transport number and electronic transport number calculated for this

Table 3.3**Heat of transport obtained from the thermoelectric power studies.**

Series 1		Series 2		Series 3	
x	Heat of transport \dot{q}_{Ag^+}	x/y	Heat of transport \dot{q}_{Ag^+}	x	Heat of transport \dot{q}_{Ag^+}
10	0.320	1.25	0.394	0.2	0.300
15	0.345	1.50	0.375	0.4	0.242
20	0.316	1.75	0.278	0.6	0.239
25	0.315	2.50	0.277	0.8	0.261
30	0.314	2.75	0.377	1.0	0.279
		3.00	0.299		

Table 3.4**Silver ion transport number evaluated for the three series.**

Series 1		Series 2		Series 3	
CdI ₂ %	t _{Ag⁺}	x/y	t _{Ag⁺}	B ₂ O ₃ %	t _{Ag⁺}
5	0.947	1.00	0.896	0.0	0.960
10	0.959	1.25	0.963	0.2	0.982
15	0.965	1.50	0.967	0.4	0.925
20	0.976	1.75	0.988	0.6	0.988
25	0.978	2.00	0.976	0.8	0.979
30	0.985	2.25	0.975	1.0	0.976
		2.50	0.978		
		2.75	0.975		
		3.00	0.982		

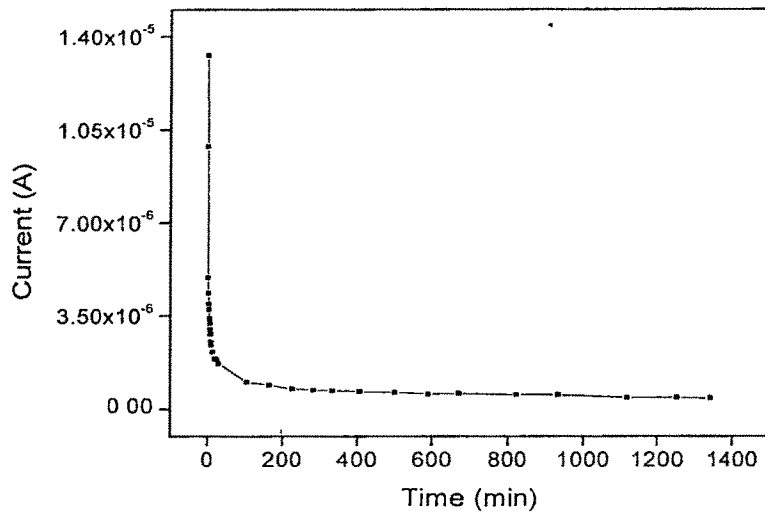


Fig.3.17. The current versus time plot obtained for the series $x\text{CdI}_2-(100-x)$ $[2\text{Ag}_2\text{O}-(0.7\text{V}_2\text{O}_5-0.3\text{B}_2\text{O}_3)]$ with $x=15$ mole % of CdI_2 composition by the Wagner's Polarization technique.

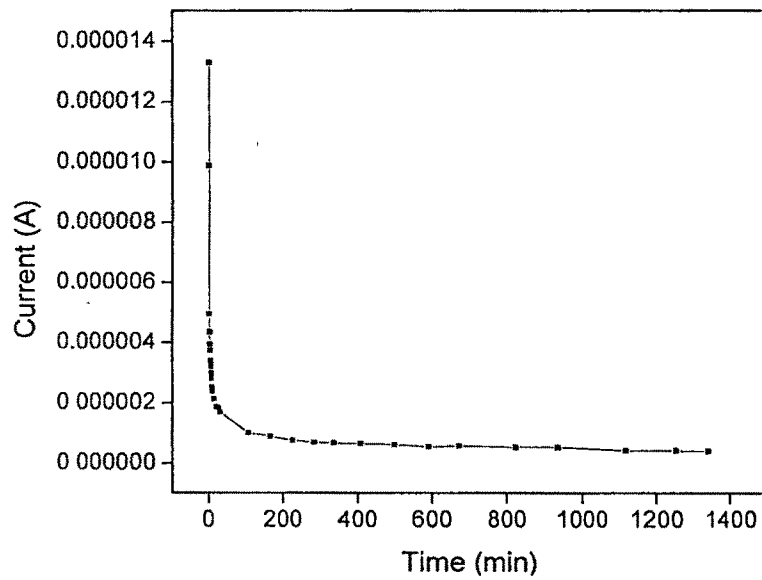


Fig.3.18. The current versus time plot for the series $20\text{CdI}_2-80[x\text{Ag}_2\text{O}-y(0.7\text{V}_2\text{O}_5-0.3\text{B}_2\text{O}_3)]$ with x/y 1.5.

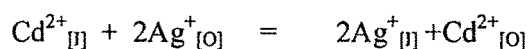
system is 0.96842 and 0.03157 respectively. Since the ionic transport number is much greater than electronic transport number, it can be easily attributed that the present glass system is an ionic conductor.

3.6.2. emf method

The silver ionic transport number t_{Ag^+} of the samples is found out by the emf method. The emf value obtained for the samples at room temperature can be compared with the corresponding theoretical value of the open circuit voltage for Ag/I₂ couple, 0.687 mV. The silver ion transport number, t_{Ag^+} of the above compositions are summarized in Tables 3.4. The silver ionic transport number t_{Ag^+} estimated are above 0.9 for the respective compositions and are nearly equal to the corresponding ionic transport number (t_{ion}) values. This means that these materials would have negligible electronic contributions to the total conductivity as compared with the ionic transport and the ionic conductivity is apparently due to Ag⁺ ions only. Table 3.4 reveals that the transport number of Ag⁺ ions is showing the increasing trend with the increase in CdI₂ and found to be nearly unity. However in the case of samples with x/y=1, x=0.4 the ionic transport number is found to be 0.896, 0.925 respectively, thus indicating mixed conduction probably due to the increased electronic contribution to the total electrical conductivity. It is evident that Ag⁺ ions are the majority charge carriers in the CdI₂ doped silver oxysalt system and the remaining contribution may arise due to the migration of Cd²⁺ ions and electrons. The occurrence of silver ionic conduction in the mixed system CdI₂-Ag₂O-V₂O₅-B₂O₃ is quite similar to that of other CdI₂ [50] and CuI [51] doped systems.

3.7. Pearson's theory of HSAB

The high silver transport numbers measured from the presently studied samples by Wagner's polarization method as well as by emf method and the high conductivity (discussed in chapter 4) may be due to the result of the reciprocal role of Cd^{2+} ions in the $\text{Ag}_2\text{O-V}_2\text{O}_5\text{-B}_2\text{O}_3$ matrix. It has been observed from the characterization studies that the formation of AgI in the system and is due to an exchange reaction taking place in the glassy matrix. During melting, Cd^{2+} from the iodine environment seems to go to the oxygen environment and Ag^+ from the oxygen environment seems to move to the iodine environment to form AgI. It can be represented as



where the subscript [I] indicates the iodine environment and [O] indicates the oxygen environment. This type of exchange reaction may be explained on the basis of softness of the Lewis acids and Lewis base [52,53]. All cations are Lewis acids and all anions are Lewis bases. A salt is an acid-base complex. Most inorganic compounds in the forms of solid, liquid and gases are examples of acid-base complexes. The complexes will be held by ionic forces when difference in the energy between frontier orbitals of the acid and base is large [32]. Pearson classified Lewis acids and Lewis bases as hard, borderline or soft.

H^+ , Li^+ , Na^+ , K^+ , Be^{2+} , Mg^{2+} , Ca^{2+} , Al^{3+} , Si^{4+} , I^{5+} , I^{7+} etc (hard acids)

Cu^+ , Ag^+ , Au^+ , Tl^+ , Hg^+ , Cs^+ , Pd^{2+} , Cg^{2+} , Hg^{2+} , I^+ , Br^+ , O , Cl , Br , I etc (soft acids)

Fe^{2+} , Co^{2+} , Ni^{2+} , Cu^{2+} , Zn^{2+} , Sn^{2+} , Pb^{2+} , Sb^{3+} , SO_2 , NO^+ etc (border line acids)

H_2O , OH^- , F^- , Cl^- , CO_3^{2-} , NO_3^- , ROH , R_2O , NH_3 , N_2H_4 etc (hard base)

$R_2S, RSH, I^-, SCN^-, CN^-, RNC, CO, C_2H_4, C_6H_6, H^-, R^-$ etc (soft base)

$C_6H_5NH_2, C_3H_5N, N^{3-}, Br^-, NO^{2-}, SO_3^{2-}, N_2$ (border line bases)

According to Pearson's hard soft [Lewis] acid base (HSAB) principle:

Hard [Lewis] acids prefer to bind to hard [Lewis] bases and Soft [Lewis] acids prefer to bind to soft [Lewis] bases.

From the above classification it is possible to deduce the hardness sequence, $H^+ > Li^+ > Na^+ > Cu^+ > Ag^+$ for monovalent ions and $Pb^{2+} \sim Cd^{2+} > Hg^{2+}$ for divalent ions. Since CdI_2 is an intermediate acid, the soft acid Ag^+ and soft base I^- prefer to form AgI clusters resulting in high silver ion transport number or conductivity. It is therefore possible that when CdI_2 is mixed with the salt ($Ag_2O-V_2O_5-B_2O_3$), AgI would be formed in agreement with the above principle. It is quite probable that during the melting process, initially Ag_2O decomposes into metallic silver and oxygen. Metallic silver released from Ag_2O could possibly be involved in the exchange reaction with CdI_2 thus forming AgI and unreacted metallic silver may be present as small traces in some samples, as revealed by XRD analysis. Similar ion exchange have been observed by many workers [3, 54-58]. These observations are in good agreement with the HSAB principle.

3.8. Summary

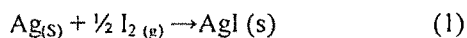
In this chapter the characterization studies of the three series of the system $CdI_2-Ag_2O-V_2O_5-B_2O_3$ are presented. X-ray diffractogram of the first series shows that the samples with $x=15$ to 25 % CdI_2 doped systems shows featureless x-ray pattern, 5 and 10 mole% CdI_2 doped systems show an amorphous background with a peak due to the agglomeration of Ag_2O and 30 mole% CdI_2 doped system shows an amorphous background with peak

due to β -AgI. In the second series, the limit of glass formation has been set at $1.5 \leq x/y \leq 3$ among the samples prepared in the different x/y ratios from 1 to 3 in steps of 0.25. In the third series, all the samples show the agglomeration of Ag_2O , traces of AgI and metallic Ag and some unidentified phases. This may be due to undissolved Ag_2O and AgI traces or insufficient quenching rate achieved for amorphisation. The glass transition temperature of the glasses decreases with increase of dopant concentration in the first series whereas in the second and third series, T_g is independent of modifier to former (x/y) ratio and with the former amount (x). This means that T_g depends mainly on the dopant concentration in the present systems. Infrared absorption spectra show that the glass network is not affected by the addition of the dopant content in the first series. In the second series, the increasing addition of Ag_2O to the system brings out the structural changes with composition and the transformation of BO_3 units to BO_4 and VO_5 to VO_4 units and observed the corresponding shift in the corresponding band towards the lower wave number. In the third series, where V_2O_5 is replaced by the B_2O_3 to the system brings the changes due to the presence of constant amount of Ag_2O . Hence, it is the modifier Ag_2O , not the dopant which is responsible for any structural changes brought in the glass system. Thermo electric power studies show the θ value obtained is negative and arises due to the motion of Ag^+ ions in thermal gradient. The heat of transport obtained from the TEP plot is comparable to the activation energies obtained from the conductivity plot. The ionic transport number found out from Wagner's polarization method and emf method is almost unity. The high silver ionic transport number observed, even if the silver vanadoborate system is doped with CdI_2 , is due to the formation of AgI clusters in accordance with the theory of hard and soft acids and bases.

Appendix [59]

Calculation of EMF of Ag/I₂ couple

The cell reaction of the Ag/AgI/I₂ system is given by



where I_{2(g)} is iodine in the vapour phase, Ag_(s) and AgI_(s) are solid silver and silver iodide respectively. The EMF, E of the system can be calculated from the familiar expression

$$E = -\Delta G/F + (RT/2F) \ln P_{\text{I}_2} \quad (2)$$

where ΔG is the increase in the free energy associated with the reaction given in eqn.1, P_{I₂}, the vapour pressure of iodine and other symbols have their usual meanings. P_{I₂} can be evaluated by

$$\ln P_{\text{I}_2} = -\Delta G_{\text{I}_2}/RT \quad (3)$$

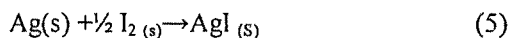
where ΔG_{I₂} is free energy increase

$$\text{I}_{2(s)} = \text{I}_{2(g)}$$

Combination of eqn. 2 and 3 leads to

$$E = -\Delta G/F - \Delta G_{\text{I}_2}/2F \quad (4)$$

Where ΔG + ΔG_{I₂}/2 is the free energy increase of



$$\Delta G + \frac{1}{2}\Delta G_{\text{I}_2} = -14400 + 8.27 \times T \log T - 6.3 \times 10^{-3} T^2 - 23.4T \quad (6)$$

Table gives the EMF values calculated from eqn.6

Table 1 - OCV of the cell at various temperatures.

Temperature (°C)	Calculated voltage (mV)
-75.8	673.5
-17.5	681.5
1.8	684.1
20.0	686.5
30.0	687.9
40.0	689.3
50.0	690.7
60.0	692.0

References

1. Beyeler H.U, Bruesch P and Hibma T, *Phys. Rev. B* 18 9 (1978) 4570.
2. Magistris A, Chiodelli G and Duclot M, *Solid State Ionics* 9/10 (1983)611.
3. Suresh Kumar R and Hariharan K, *Solid State Ionics* 104 (1997) 227.
4. Sastry M.C.R, Rao K.J, *Solid State Ionics* 51 (1992) 311.
5. Venkateswarlu M, Narasimha Reddy K, Rambabu B and Satyanaraya N, *Solid State Ionics* 127 (2000) 177.
6. Karthikeyan A, Govindaaraj G, Satyanarayana N and Venkateswarlu M, *Mate. Sci. Eng.B* 13 (1992) 295.
7. Chowdari B.V.R, Gopalakrishnan R, Goh S.H and Tan K.L, *J. Mate. Sci.* 23 (1988) 1248.
8. Chiodelli G, Pezzati E, Baldeno P and Martin S.W, *Solid State Ionics* 18&20 (1986) 426.
9. Kaushik R and Hariharan K, *Solid State Commun.* 63 10 (1987) 925.
10. Chiodelli G and Magistris A, *Solid State Ionics* 18&19 (1986) 356.
11. Willard H.H, Meritt L.L and Dean J.A. Jr., *Instrumental methods of Analysis*, Affiliated East Cost Press Pvt. Ltd, New Delhi , Fourth Edition (1965) 124.
12. Chatwal G and Anand S, *Spectroscopy (Atomic and Molecular)* eds. by Arora M and Puri S, Himalaya Publishing House, Bombay (1983) 39.
13. Kurjain C.R and Sigety E.A, *Physics Chem. Glasses*, 9 (1968) 73.
14. Kurjain C.R, *J. Non-Cryst. Solids* 3 (1970) 157.
15. Bansal T.K and Mendiratta R.G, *Physics Chem. Glasses* 28, 6 (1987) 242.
16. Nishida T and Takashima Y, *J. Non-Cryst. Solids* 94 (1987) 229.
17. Sanad A.M, Kashif I, El-Sharkawy A.A, El-Saghir A.A and Farouk H, *J. Mate. Sci.Lett.*2 (1983) 649.
18. Culea E. Nicula A.I., Bratu I, *Phys. Stat. Sol. (a)* 83 (1984) k15.
19. Hogarth C.A and Ahmed M.M, *J. Mat. Sci. Lett.* 2 (1983) 649.
20. Kanchan D.K and Panchal H.R, *Tr. J. Phys.* 22 (1998) 989.
21. Kamitsos E.I, Karakassides M.A, Chryssikos G.D, *Phy. Chem. Glasses* 28 5 (1987) 203.
22. Krogh- Moe J, *Physics Chem .Glasses* 6,2 (1965) 46.
23. Dimitrov V, Diitriev Y and Mihailova V, *Monatshefte fur Chemie* 114 (1983) 669.
24. Bachman H.G, Ahmed F.R. Barner W.H, *Z. Krstallogh* 115 (1961) 110.
25. Anderson S, Bohon R.L and Kimpton D.D, *J. Am. Ceram. Soc.* 38 (1955) 370.
26. Jellyman P.E and Proctor J.P, *Trans. Soc. Glass; Technol* 39 (1955) T173.
27. Dimitrov V, Dimitriev Y, *J. Non-Cryst. Solids* 122 9(1990) 133.

28. Dimitriev Y, Ivanova I, Dimitrov V, Lackov L, *J. Mate. Sci.* 21 (1986) 142.
29. Arof A.K. *J. Power Sources* 45 (1993) 255.
30. Dalba G, Fornasini P, Rocca F, *J. Non-Cryst. Solids* 101 (1998) 70.
31. Vogel W and Kriedle N, *Chemistry of Glasses*, Published by the American Ceramic Soc. Inc. Columbus, Ohio (1985).
32. Suresh Kumar R, .PhD Thesis, IIT Madras (1999).
33. Shahi K and Chandra S, *Phys. Stat. sol. (a)* 28 (1975) 653.
34. Hariharan K and Kaushik R, *Mate. Chem. Phys.* 15 (1986) 447.
35. Girvin S.M, *J. Solid State Chem.* 25 (1978) 65.
36. Hariharan K, Tomy C.V and Kaushik R, *J. Mate. Sci. Lett.* 4 (1985) 1379.
37. Scrosati B, Papalov F and Pistoia G, *J. Electrochem. Soc.* 122 (1975) 339.
38. Murugesamoorthi K.A and Radhakrishna S, *J. Mate. Sci. Lett.* 4 (1985) 801.
39. Shahi K, *Phys. Stat. Sol. (a)* 41 (1977) 11.
40. Allnatt A.R and Rice S.A, *J. Solid State Chem.* 33 (1960) 573.
41. Rice M.J and Roth W.L, *J. Solid ate Chem.* 4 (1972) 294.
42. Avasthi M.N, *Phys. Stat. sol. (a)* 71 (1982) KI77.
43. Owens B.B and Argue G.R, *Science* 157 (1967) 308.
44. Wagner C, *Z. Electrochem.* 60 (1956) 4.
45. Wagner C, *Z. Electrochem.* 63 (1959) 1027.
46. Danforth W.E md Bodine J.H., *J. Franklin Inst.* 260 (1955) 467.
47. Wagner J.B and Joshi A.V, *J. Phys. Chem. Solids*, 33 (1972) 205.
48. Schoonman J and Macke A.J.H, *J. Solid State Chem.* 5 (1972) 105.
49. Schoonman J and Dijkman F.G, *J. solid State chem.* 5 (1972)111.
50. Suthanthiraraj S.A and Ganeshkumar A.C, *J. Mate. Sci. Lett.* 17 (1998) 1569.
51. Viswanathan A, Suthanthiraraj S.A, *Solid State Ionics* 62 (1993) 79.
52. Pearson R.G, *J. Am. Chem. Soc.*, 85 (1963) 3533.
53. Pcarson R.G, *Science*, 151 (1966) 172.
54. Hariharan K and Suresh Kumar R. *Solid State Ionics: Materials and Applications*, eds Chowdari B.V.R et. al., world Scientific, Singapore (1992) 533.
55. Sureshini A.M and Hariharan K, *Mater. Res. Bull.* 27 (1992) 9.
56. Chandrasekhar V.G and Suthanthiraraj S.A, *Solid State Ionics* 62 (1993) 61.
57. Malugani J.P, Mercier R and Tachez M, *Solid State Ionics* 21 (1986) 131.
58. Rivolta B, Bonino F and Scrosati B, *Mater. Chem. Phys.* 19 (1988) 557.
59. Gopalakrishnan K, PhD Thesis, National University Singapore (1989).